Laser and Particle Beams (2016), *34*, 506–512.

doi:10.1017/S0263034616000392

Investigation of ionization speed in field ionization with laser–plasma interaction

Y. TIAN,[1] X. JIN,[1] W. YAN,[1] X. GU,[1] J. YU,[1,2] J. LI,[1] AND B. LI[1]

[1]University of Electronic Science and Technology of China, Chengdu, China
[2]Imperial College London, London, UK

(RECEIVED 20 April 2016; ACCEPTED 31 May 2016)

Abstract

The effects of target density and laser intensity on ionization speed are studied in this paper by 1D3V particle-in-cell simulations, where the field ionization of single atom is involved basing Ammosov-Delone-Krainov model in the form of Penetrante and Bardsley. To consider the ionization speed, the evolution of plasma density for the helium target, particularly, the ion density change rate near the target front surface, are discussed. The results show that not only the laser intensity, but also the target density will affect field ionization and further affect the plasma formation. This work will be helpful for further understanding of plasma formation in intense laser pulse. Also, it may be benefit for the setup of initial parameters before the simulation of laser–plasma interaction.

Keywords: Field ionization; Plasma formation; PIC; Ionization speed; Laser–plasma interaction

1. INTRODUCTION

The rapid development of ultrahigh-intensity ($I > 10^{18}$ W/cm^2) short-pulse laser, whose intensity greatly exceeding the strength required to induce atomic-scale relativistic behavior, has greatly motivated the discovery of laser–plasma interaction. Many researches, including fast electron production and transport during the interaction (Cohen *et al*., 2010; Sakagami *et al*., 2012; Fox *et al*., 2013), ion acceleration driven by intense laser pulse (Lefebvre *et al*., 2010; d'Humières *et al*., 2013; Macchi *et al*., 2013), have been extensively studied as the potential applications in fast ignition of inertial confinement fusion (JinQing *et al*., 2012; Robinson *et al*., 2014) and other related fields (Daido, 2012; Jinqing *et al*., 2012). In laser–plasma interaction, ionization plays a critical role on plasma formation. And the formed plasma will further affect the laser–plasma interaction (Lichtenberg, 2005). Hence, understanding the whole interaction process including ionization is critical for the researches on laser–plasma interaction and particle acceleration.

In modeling the laser–plasma interaction with particle-in-cell (PIC) code, the target is usually assumed to be pre-ionized plasma. This is because the ionization process generally has finished before the main laser pulse reaching the target (Esarey *et al*., 2009). However, ionization will affect the propagation of the main laser pulse in the plasma and the subsequent processes, including electron impact ionization, Coulomb collision, hot electron production, scattering, and so on. Thus, assuming pre-ionized plasma will ignore many interesting physics phenomena. It is necessary to study the ionization process in laser–plasma interaction. Effects of field ionization on the acceleration process (McGuffey *et al*., 2010; Psikal *et al*., 2011, 2012) and effects of laser pulse on field ionization process (Petrov *et al*., 2009) have been considered in the past. However, to the best of our knowledge, the effect of target density, which is also important to understand the whole interaction process, has not been analyzed before.

In this paper, we studied the effects of target density and laser pulse intensity on field ionization with PIC/Monte Carlo collisional (MCC) simulations using a relativistic and fully electromagnetic 1D3V PIC/MCC code Bumblebee (Xiaolin *et al*., 2015). The Ammosov-Delone-Krainov (ADK) rate formula (Ammosov & Krainov, 1986) is applied to model the field ionization process. The helium (He) material is used in the simulation to discuss the physical issues. The field ionization model is illustrated in Section 2. To illustrate the effect of target density, we will present the ion density and its change rate for different target densities at a given laser intensity in Section 3. The results of different laser intensities are compared in Section 4.

Address correspondence and reprint requests to: X. Jin, School of Physical Electronics, University of Electronic Science and Technology of China, Chengdu 610054, China. E-mail: jinxiaolin@uestc.edu.cn

2. DYNAMICS MODEL OF FIELD IONIZATION

The field ionization model has been implemented in Bumblebee. Ionization rate is given by the ADK formula (Kemp *et al.*, 2004)

$$\omega_{\mathrm{i}} = 6.6\times10^{16}\frac{Z^2}{n_{\mathrm{eff}}^{4.5}}\left[10.87\frac{Z^3}{n_{\mathrm{eff}}^4}\frac{E_{\mathrm{h}}}{\left|\vec{E}(t)\right|}\right]^{2n_{\mathrm{eff}}-1.5} \times\exp\left[-\frac{2}{3}\frac{Z^3}{n_{\mathrm{eff}}^3}\frac{E_{\mathrm{h}}}{\left|\vec{E}(t)\right|}\right], \tag{1}$$

where $E_{\mathrm{h}} \equiv m_{\mathrm{e}}^2 e^5 \hbar^{-4} = 5.14\times10^9\ \mathrm{V/cm}$ is the atomic field strength, e and m_{e} are the charge and mass of electron, respectively, $\hbar$ is Planck constant, $n_{\mathrm{eff}} = Z/\sqrt{W_{\mathrm{i}}/I_{\mathrm{H}}}$ is the effective main quantum number of the new produced electron by ionization (called "ionized electron" below), Z is the ion charge after ionization, W_{i} is the ionization energy for a given process, I_{H} is the ionization potential of hydrogen and $\vec{E}(t)$ is the instantaneous electric field at the position of the traced particle (ion or atom).

In order to fulfill energy conservation, energy loss of field ionization ΔW_{ion} is assumed to be equal to the electromagnetic field energy change $\Delta W_{\mathrm{field}}$ in each cell and each time step, that is, $\Delta W_{\mathrm{field}} = \Delta W_{\mathrm{ion}}$. An artificial ionization current density $\vec{J}_{\mathrm{ion}}$, which is directed along the electric field $\vec{E}(t)$, is introduced to calculate the field energy change during ionizations (Kemp *et al.*, 2004). The ionization current density is determined by

$$\int dt\int dV\vec{J}_{\mathrm{ion}}(t)\cdot\vec{E}(t) = \Delta W_{\mathrm{field}}, \tag{2}$$

where the integrals are taken over one time step and one cell, respectively. The energy loss of field ionization is given by

$$\Delta W_{\mathrm{ion}} = \sum_j w_j\left(W_{i,j}+\varepsilon_j\right). \tag{3}$$

Here $\sum_j$ is the sum over all ionization processes in one cell and one time step, w_j and $W_{i,j}$ are the weight of the ionized macro-particle (called "particle" below) and the ionization energy for the jth ionization event, respectively, ε_j is the initial kinetic energy of the ionized electron. We assume that the velocity direction of the ionized electron is parallel to that of ion and the velocity magnitude is equal to that of ion. Then the value of ε_j can be obtained. According to energy conservation, the relation between ionization current density and electric field should satisfy

$$\vec{J}_{\mathrm{ion}}(t)\cdot\vec{E}(t)\Delta t\Delta V = \sum_j w_j\left(W_{i,j}+\varepsilon_j\right), \tag{4}$$

where Δt and ΔV are the time step and the cell size in PIC simulation, respectively. Equation (4) can be deduced to

$$\vec{J}_{\mathrm{ion}}(t) = \frac{\sum_j w_j(W_{i,j}+\varepsilon_j)}{\Delta t\Delta V\left|\vec{E}(t)\right|^2}\vec{E}(t). \tag{5}$$

By adding the ionization current density to the deposited particle current density, the physical current in each cell and each time step can be obtained.

3. EFFECT OF TARGET DENSITY

3.1. Simulation model

A laser pulse of $20T$ is used in the simulations, where T is the laser period. Figure 1 gives the configurations of the laser and target. The laser wavelength is $\lambda = 0.8$ μm. The laser pulse envelope rises to peak in the first $5T$ and maintains in the next $10T$, then drops to zero in the last $5T$. The peak laser pulse intensity is given by $I\lambda^2 = a^2 1.37\times10^{18}\ \mathrm{W\,\mu m^2/cm^2}$, here a is the dimensionless maximum field amplitude. The laser is normally incident on a 30λ thick neutral target, corresponding to the blue region in Figure 1. The neutral atom density n is normalized by the critical density n_{c}, which is defined as $n_{\mathrm{c}} = \varepsilon_0 m_{\mathrm{e}}\omega^2/e^2$, ε_0 is the permittivity of free space, and ω is the laser frequency.

The ionization electric field for He^{2+} and He^{+} are 2.57×10^{11} and $1.05\times10^{11}\ \mathrm{V/m}$, respectively, which can be estimated using the formula $E_{\mathrm{i}} = (W_{\mathrm{i}}/2I_{\mathrm{h}})^2 E_{\mathrm{h}}/4i$ (Petrov *et al.*, 2009). And i represents the ion charge after ionization. The incident laser electric field amplitude ($E_{\mathrm{l}} = am_{\mathrm{e}}\omega c/e \approx 2.2\times10^{12}\ \mathrm{V/m}$) is almost 22 and 8.6 times the ionization electric field for He^{+} and He^{2+}, respectively. Therefore, the helium atom can be fully ionized if the laser interacts with the neutral target completely.

3.2. Results and discussion

The ionization rate is independent on the target density as seen in Eq. (1). However, target density affects the transport of laser pulse and further affects the field ionization process. Based on this consideration, we investigated the influences of different initial target densities on field ionization. We firstly analyzed the evolution of ion density to understand the ionization process. After that, to illustrate the ionization speed, the space-averaged ion density and the ion density change rate of He gas target, particularly near the target front surface

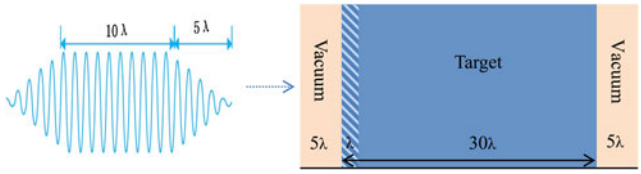

Fig. 1. Laser and target configuration.

https://doi.org/10.1017/S0263034616000392 Published online by Cambridge University Press

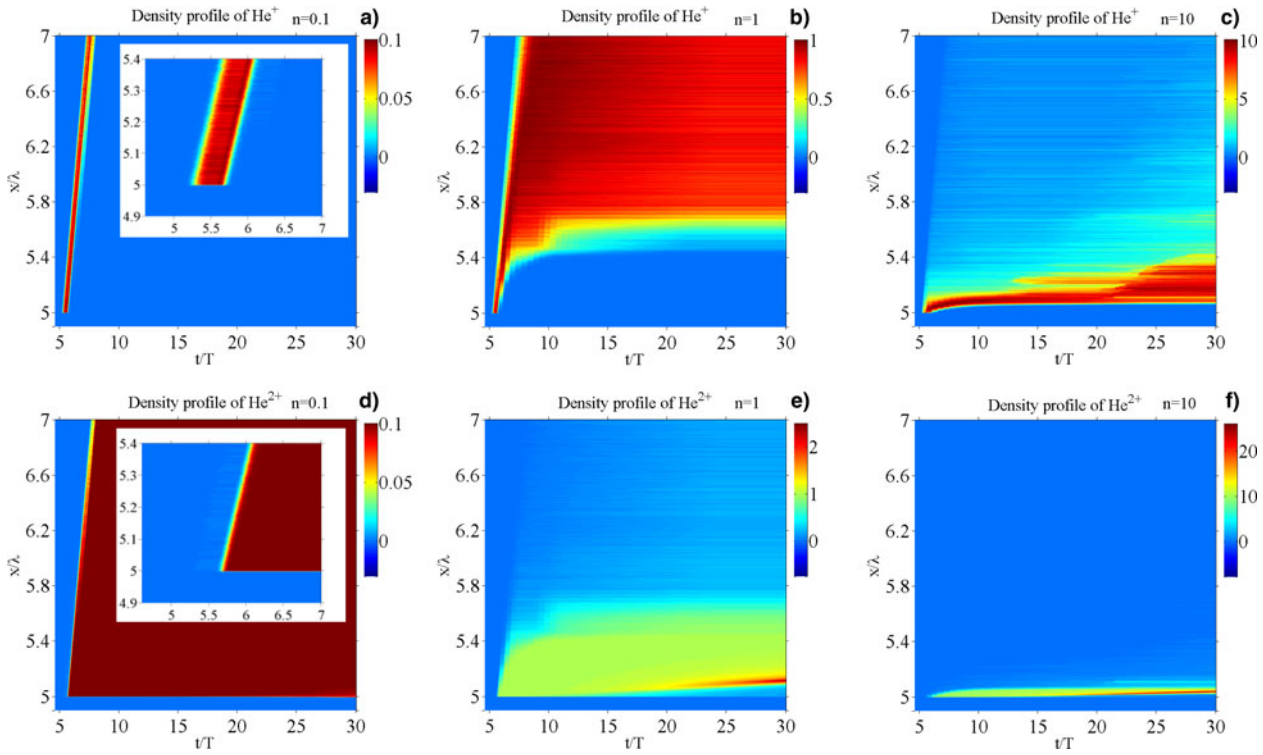

Fig. 2. The spatio-temporal evolutions of He^+ for (a) $n = 0.1$; (b) $n = 1$; (c) $n = 10$. The spatio-temporal evolutions of He^{2+} (bottom) for (d) $n = 0.1$; (e) $n = 1$; (f) $n = 10$. The color bar represents the particle number density.

(represented by a 1λ region, see the shadowed region of Fig. 1), were discussed.

We considered different He gas target densities ($n = 0.1$, $n = 1$ and $n = 10$) with a constant laser intensity $a = 0.5$. The neutral atom density n is normalized by the critical density n_c. The spatio-temporal evolutions of He^+ and He^{2+} density are shown in Figure 2. Two factors affect the ionizations of He atoms, one is the laser field, and the other is the electrostatic field caused by the transport of energetic electrons.

Firstly, we will discuss the effect of laser field. He^+ appearance and disappearance processes are clearly shown in Figure 2a. At the beginning, no ionization happens, as the laser field is not strong enough to ionize the target. Shortly after the laser intensity reaches the field-ionization intensity threshold (Posthumus *et al.*, 1995) ($t \sim 5.2T$, see the inset of the figure), He^+ ions begin to appear. It should be noted that the laser intensity does not reach the threshold when the laser just arrives at the target ($t = 5T$), because there is vacuum region of 5λ on the left of the simulation region and the laser pulse envelope is not a flat-top at the first $5T$ (see Fig. 1). He^+ is ionized to He^{2+} as the laser transmitting into the target after $5.2T$. As a result, He^+ ions decrease with time, as seen in Figure 2a. And He^{2+} ions are observed at $x \approx 5.2\lambda$ with the density continuously increasing from 5.6 to $5.7T$, then the density of He^{2+} maintains at $0.1n_c$ throughout the simulation, see Figure 2d. When atom density is approximately equal to n_c ($n = 1$), He^+ almost cannot be ionized to He^{2+} behind $x = 5.7\lambda$ (Fig. 2e), so most He^+ ions remain unchanged (Fig. 2b) as only a small part of laser energy could transport into the target. For the case of $n = 10$, the laser could only propagate into the target for a short distance (nearly the plasma skin length). As a result, the laser pulse is stopped at such high density. Thus, only a very thin target layer can be ionized at $n = 10$ (right column of Fig. 2). In conclusion, the thickness of the ionized region is determined by laser parameters and target density.

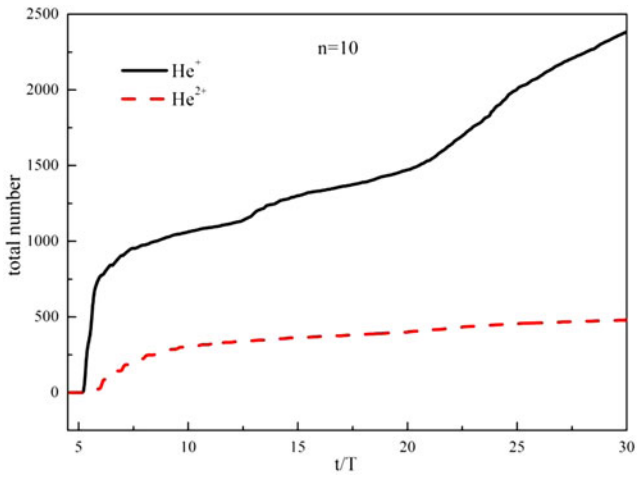

Fig. 3. The temporal evolutions of He^+ and He^{2+} numbers.

After the laser irradiation is over, the ions are affected by the electrostatic field caused by the transport of energetic electrons. As can be seen in the right two plots of Figure 2, He^+ ions increase with time till the atoms being fully ionized

https://doi.org/10.1017/S0263034616000392 Published online by Cambridge University Press

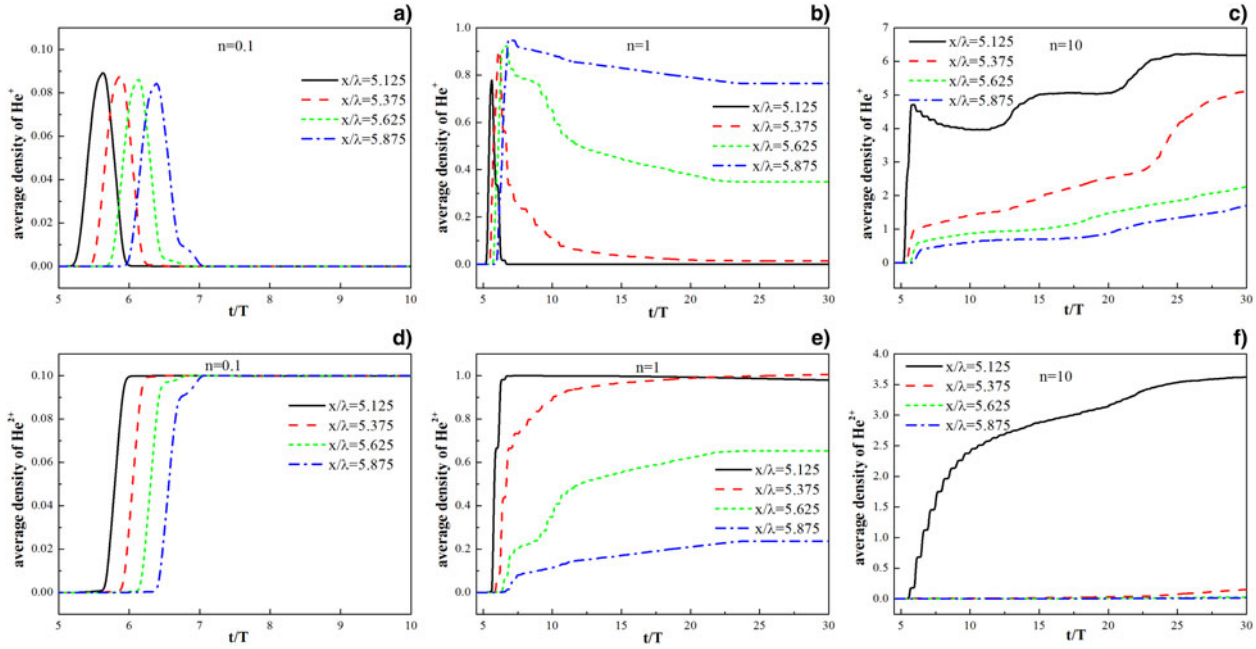

Fig. 4. The temporal evolutions of He^+ average density for (a) $n = 0.1$; (b) $n = 1$; (c) $n = 10$. The temporal evolutions of He^{2+} average density (bottom) for (d) $n = 0.1$; (e) $n = 1$; (f) $n = 10$.

to He^+ at density ~10, even no incident laser after $t = 25T$, which is different from the case of He^{2+}. Ionized electrons are accelerated forward by laser pulse after the generation of He^+, resulting in the formation of space-charge field inside the target. The space-charge field further ionizes He atoms to He^+ after the laser irradiation is over, while the field amplitude has not reached the requirement for second ionization. Thus, the region of He^+ is much larger than that of He^{2+}. Moreover, we can find a small region with high density of He^{2+} ($n \sim 28$) in Figure 2f. To find out the reason of such high density, we plot the temporal evolutions of the total particle numbers in the simulation region in Figure 3. We can clearly see that the total number of He^{2+} nearly sustains constant for $n = 10$. Therefore, the high density of He^{2+} is resulted from ions bunching, which is caused by electrostatic field push.

We note that the target front surface (see the shadowed region of Fig. 1) is the initial location of the ionization process and the most intense part of the laser–plasma interaction. Additionally, the tendency of ion density versus time shares similar characteristic at different positions for low target density (see Fig. 2a, 2d). Hence, the space-averaged ion densities at four typical positions near the target front surface, which are calculated over an interval of 0.25λ and presented in Figure 4, have been obtained to analyze the ionization process. For clarity, the averaged ion density is

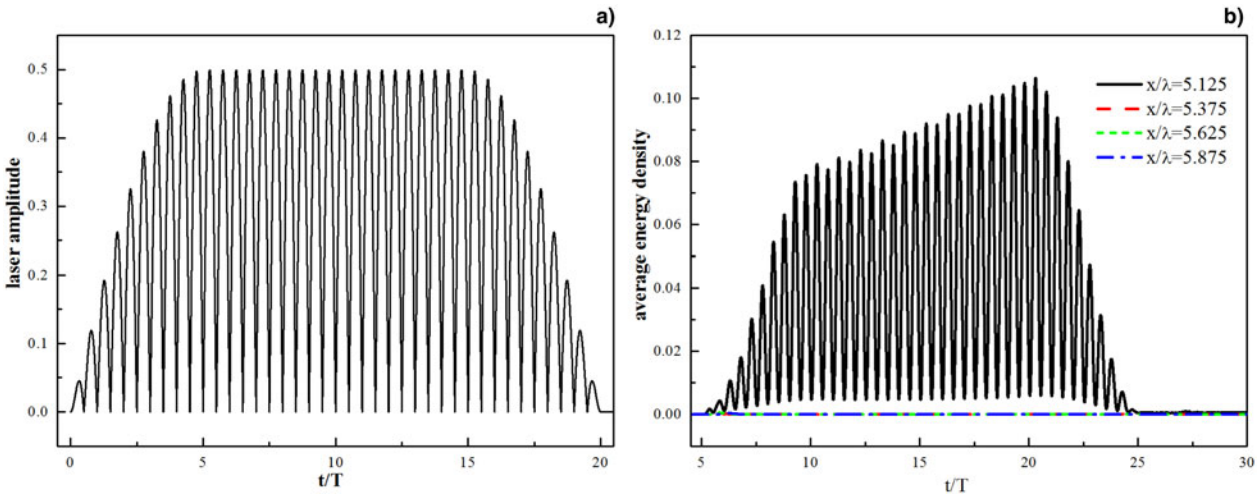

Fig. 5. The temporal evolutions of (a) the laser pulse amplitude and (b) the field amplitude with the density $n = 10$.

https://doi.org/10.1017/S0263034616000392 Published online by Cambridge University Press

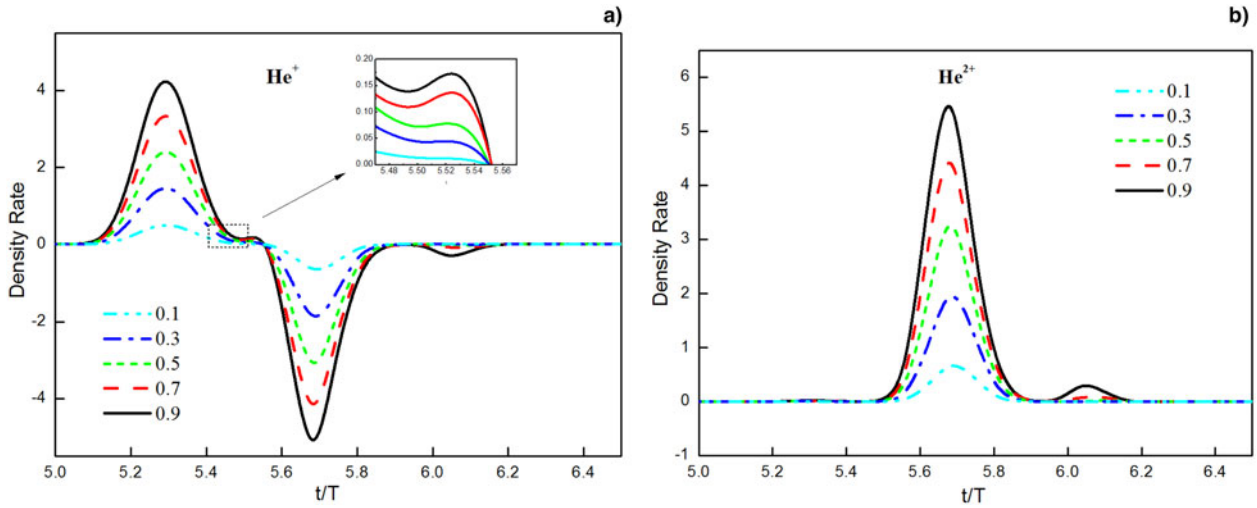

Fig. 6. The ion density change rates of (a) He^{+} and (b) He^{2+} for different initial target densities as $x < 0.1\lambda$.

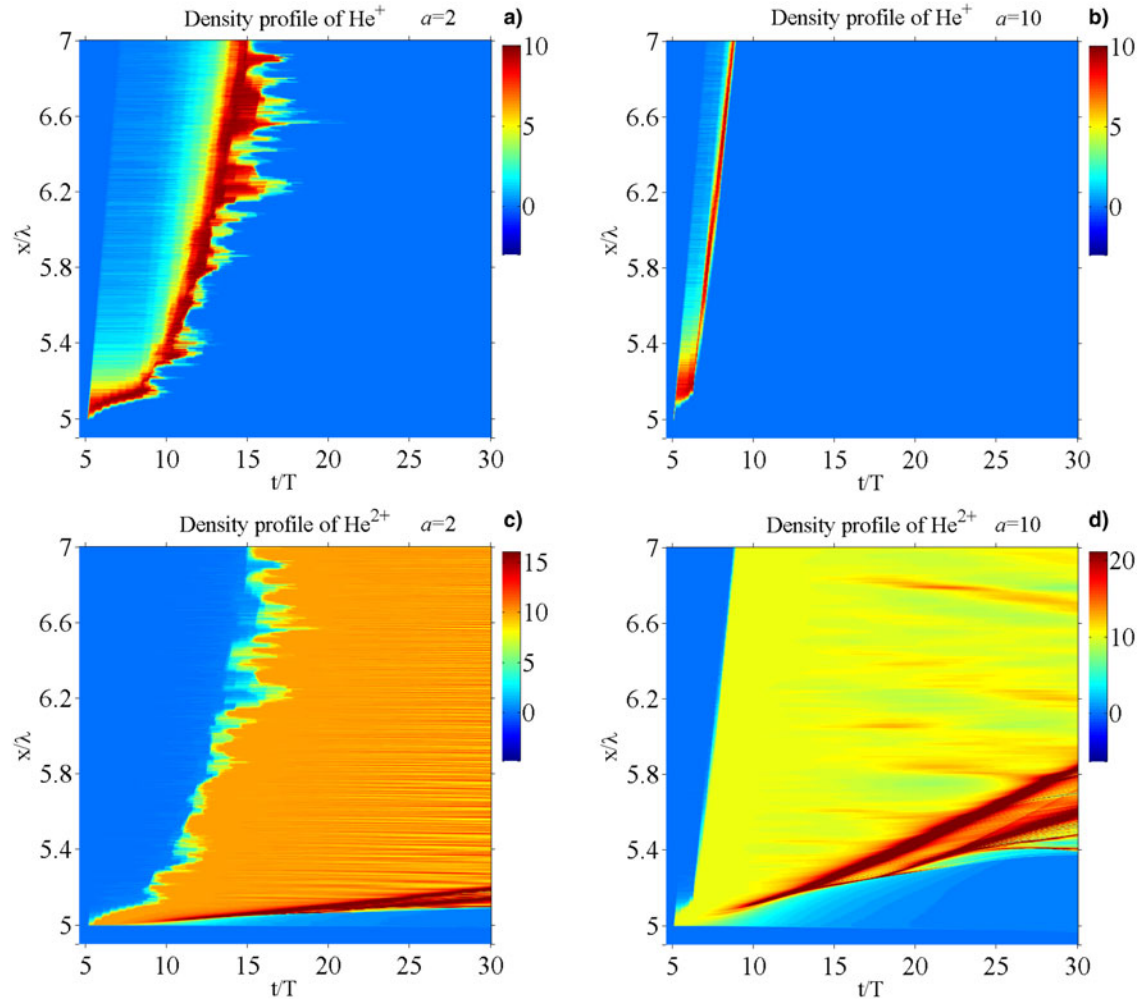

Fig. 7. The spatio-temporal evolutions of He^{+} for (a) $a = 2$; (b) $a = 10$. The spatio-temporal evolutions of He^{2+} (bottom) for (c) $a = 2$; (d) $a = 10$. The color bar represents the number particle density.

https://doi.org/10.1017/S0263034616000392 Published online by Cambridge University Press

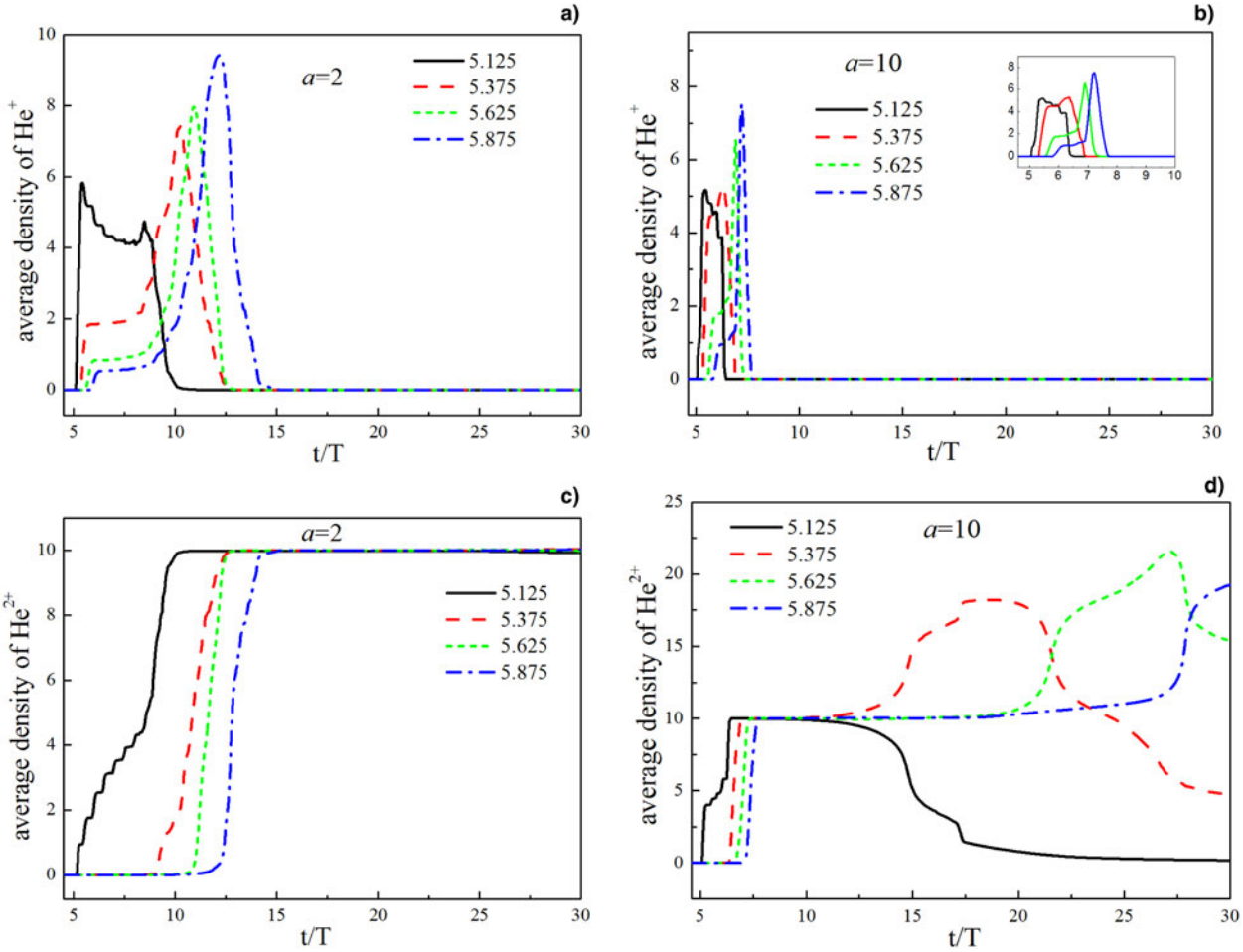

Fig. 8. The temporal evolutions of He^+ average density for (a) $a = 2$; (b) $a = 10$. The temporal evolutions of He^{2+} average density (bottom) for (c) $a = 2$; (d) $a = 10$.

plotted only before $10T$ for $n = 0.1$ because of its unchanged tendency after $10T$.

As we can see, the averaged ion densities for various target densities in Figure 4 are significantly different. For He^+ (Fig. 4a–c), the averaged density becomes difficult to decrease with increasing initial target density after it reaches the peak value, and even increase with time for $n = 10$. The reason is the same as the explanation of Figure 2, that is, the higher the target density is, the less the laser energy could transport into the target. Hence, He^+ is difficult to be ionized to He^{2+}. For He^{2+} in Figure 4f), due to the effect of skin depth, He^+ ions can be still ionized to He^{2+} ions within the skin length for $n = 10$. Therefore, we can obviously observe a black line whose peak value is higher than other lines in Figure 4f. In summary, the results in Figure 4 are generally consistent with the analysis of Figure 2.

In addition, one can see from Figure 4f that the black line increases as a stair-step shape, and the oscillation frequency is twice of the laser frequency. This is probably caused by the injected laser with a sin-shaped ramp amplitude at the laser pulse front. The incident laser amplitude profile with time is shown as Figure 5a, and the space-averaged total field energy ($E^2 + B^2$, E and B are the total electric field and magnetic field, and normalized by $m_e\omega c/e$ and $m_e\omega/e$, respectively) versus time in the plasma region is shown in Figure 5b. The black lines ($x = 5.125\lambda$) in Figures 5b and 4f display the same stair-step shape, which means the laser field stimulates He^{2+} density distribution of $x = 5.125\lambda$ in Figure 4f. Compared with the result of $x = 5.125\lambda$, the space-averaged field energy for the other three curves in Figure 5b is almost equal to zero. For the cases of $n = 1$ and $n = 10$ (corresponding target density $n \geq n_c$), atoms at the target front are ionized quickly. The ion density consequently increases with time and becomes higher than critical density n_c, as a result, the laser can hardly propagate into the target. As the laser field has been stopped by high-density plasma, no effective ionization events take place inside the target except the target front surface.

Figure 6 shows the temporal evolution of the ion density change rate for He^+ and He^{2+} with lower initial target density $n < n_c$ near the target front surface ($x < 0.1\lambda$). The ion density change rate is calculated by $(n_k - n_{k-1})/\Delta t$, where n_k is the averaged density for the kth time step. In summary, the ion density change rate changes much faster with increasing target density for $n < n_c$.

https://doi.org/10.1017/S0263034616000392 Published online by Cambridge University Press

4. EFFECT OF LASER PULSE INTENSITY

To observe the effect of laser pulse intensity on ionization, the target density is fixed to $n = 10$ with laser intensity varying from $a = 2$ to $a = 10$ in this section. Figure 7 shows the spatio-temporal density evolutions of He^+ and He^{2+} at different laser intensities. In laser–plasma interaction, the electron ponderomotive temperature T_e is proportional to the square root of the laser intensity I. Therefore, higher laser intensity results in higher temperature of forward electron and consequently larger space-charge field, which ionizes He^+ to He^{2+}. Hence, larger ionized region is formed, which can be found from He^+ and He^{2+} density distributions for different laser intensities in Figures 2c, 2f and 7. Also, we can find that high-density region of He^{2+} for $a = 2$ and $a = 10$ (Fig. 7c, 7d) is larger than the case of $a = 0.5$ (Fig. 2f). The formation of such high density has been discussed above.

The space-averaged ion density averaged over an interval of 0.25λ at different positions is shown in Figure 8. The results in Figure 8 are consistent with the analysis of Figure 7. Furthermore, the comparison of averaged density of He^+ in Figures 4c, 8a, and 8b indicates that ionization process is much faster for higher laser intensity.

5. CONCLUSIONS

Plasma formation due to field ionization has been studied with 1D3V PIC/MCC code Bumblebee in this paper. The effects of target density and laser intensity on ionization have been discussed in detail. The simulation results indicate that the laser intensity will affect field ionization as expected. Besides, the target density will also affect field ionization. For the case of $n \geq n_c$, an ionization region is formed near the target front surface. While for the case of $n < n_c$, the ionization speed increases with the initial target density. In addition, the greater the laser intensity is, the faster the ionization speed and the larger the ionization region will be. This work may be benefit for the understanding of plasma formation with intense laser pulse and the setup of initial plasma distribution before numerical modeling of the laser–plasma interaction.

ACKNOWLEDGMENT

This work was supported by National Natural Science Foundation of China (Grant Nos 61201003 and 61301054).

SUPPLEMENTARY MATERIAL

The supplementary material for this article can be found at http://dx.doi.org/10.1017/S0263034616000392.

REFERENCES

Ammosov, M.V., Delone, N.B. & Krainov, V. (1986). Tunnel ionization of complex atoms and atomic ions in an alternating electromagnetic field. *Sov. Phys. JExp. Theor. Phys*. **64**, 1191–1194.

Cohen, B.I., Kemp, A.J. & Divol, L. (2010). Simulation of laser–plasma interactions and fast-electron transport in inhomogeneous plasma. *J. Comput. Phys*. **229**, 4591–4612.

Daido, H. (2012). Review of laser-driven ion sources. *Rep. Prog. Phys*. **75**, 056401.

d'Humières, E., Brantov, A., Bychenkov, V.Yu. & Tikhonchuk, V.T. (2013). Optimization of laser-target interaction for proton acceleration. *Phys. Plasmas* **20**, 023103.

Esarey, E., Schroeder, C.B. & Leemans, W.P. (2009). Physics of laser-driven plasma-based electron accelerators. *Rev. Mod. Phys*. **81**, 1229–1285.

Fox, T.E., Robinson, A.P.L. & Pasley, J. (2013). Strong shock generation by fast electron energy deposition. *Phys. Plasmas* **20**, 122707.

Jinqing, Y., Weimin, Z., Lihua, C., Zongqing, Z., Leifeng, C., Lianqiang, S., Dongxiao, L., Xiaolin, J., Bin, L. & Yuqiu, G. (2012). Enhancement in coupling efficiency from laser to forward hot electrons by conical nanolayered targets. *Appl. Phys. Lett*. **100**, 204101.

Kemp, A.J., Pfund, R.E.W. & Meyer-ter-Vehn, J.r. (2004). Modeling ultrafast laser-driven ionization dynamics with Monte Carlo collisional particle-in-cell simulations. *Phys. Plasmas* **11**, 5648.

Lefebvre, E., Gremillet, L., Lévy, A., Nuter, R., Antici, P., Carrié, M., Ceccotti, T., Drouin, M., Fuchs, J., Malka, V. & Neely, D. (2010). Proton acceleration by moderately relativistic laser pulses interacting with solid density targets. *New J. Phys*. **12**, 045017.

Lichtenberg, M.A.L.A.J. (2005). *Principles of Plasma Discharges and Materials Processing*. New York: John Wiley & Sons.

Macchi, A., Borghesi, M. & Passoni, M. (2013). Ion acceleration by superintense laser-plasma interaction. *Rev. Mod. Phys*. **85**, 751–793.

McGuffey, C., Thomas, A.G.R., Schumaker, W., Matsuoka, T., Chvykov, V., Dollar, F.J., Kalintchenko, G., Yanovsky, V., Maksimchuk, A., Krushelnick, K., Glazyrin, I.V. & Karpeev, A.V. (2010). Ionization induced trapping in a laser wakefield accelerator. *Phys. Rev. Lett*. **104**, 025004.

Petrov, G.M., Davis, J. & Petrova, T. (2009). Ionization dynamics of high-intensity laser–target interactions. *Plasma Phys. Control. Fusion* **51**, 095005.

Posthumus, J.H., Frasinski, L.J.F., Giles, A.J. & Codling, K. (1995). Dissociative ionization of molecules in intense laser fields: A method of predicting ion kinetic energies and appearance intensities. *Phys. B. At. Mol. Opt. Phys*. **28**, L349–L353.

Psikal, J., Klimo, O. & Limpouch, J. (2011). Field ionization effects on ion acceleration in laser-irradiated clusters. *Nucl. Instrum. Meth. A* **653**, 109–112.

Psikal, J., Klimo, O. & Limpouch, J. (2012). 2D particle-in-cell simulations of ion acceleration in laser irradiated submicron clusters including field ionization. *Phys. Plasmas* **19**, 043107.

Robinson, A.P.L., Strozzi, D.J., Davies, J.R., Gremillet, L., Honrubia, J.J., Johzaki, T., Kingham, R.J., Sherlock, M. & Solodov, A.A. (2014). Theory of fast electron transport for fast ignition. *Nucl. Fusion* **54**, 054003.

Sakagami, H., Okada, K., Kaseda, Y., Taguchi, T. & Johzaki, T. (2012). Collisional effects on fast electron generation and transport in fast ignition. *Laser Part. Beams* **30**, 243–248.

Xiaolin, J., Tao, H., Wenlong, C., Jianqing, L., Hualiang, L., Bin, L. & Zhonghai, Y. (2015). BUMBLEBEE: A 1D3V relativistic PIC/MCC software for laser-plasma interaction. *Proc. IEEE ICOPS*, Belek, Turkey.